Simulation of the Indian Ocean Dipole: a relevant criterion for selecting models for climate projections

W. Cai[1], A. Sullivan[1], T. Cowan[1], J. Ribbe[2], and G. Shi[2]

W. Cai, CSIRO Marine and Atmospheric Research, PMB 1, Aspendale, Victoria 3195, Australia. (wenju.cai@csiro.au)

[1]CSIRO Marine and Atmospheric Research, Aspendale, Victoria, Australia

[2]Department of Biological and Physical Sciences, University of Southern Queensland, Toowoomba, Australia

A multi-model average shows that 21st century warming over the eastern Indian Ocean (IO) is slower than that to the west, but with strong inter-model variations. Is the simulation of the Indian Ocean Dipole (IOD) relevant to the inter-model variations? We demonstrate that inter-model variations of this future warming are consistent with how well models simulate historical IOD properties; models with a stronger IOD amplitude systematically produce a slower eastern IO warming rate with greater future rainfall changes in IOD-affected regions. These models also produce a stronger Bjerknes-like positive feedback, involving sea surface temperatures (SSTs), winds and a shoaling thermocline in the eastern IO. As warming proceeds, models with a stronger positive feedback induce a greater response to warming-induced changes such as easterly trends associated with the Walker circulation, generating a smaller warming in the eastern IO. Simulating the present-day IOD properties is, therefore, a relevant criterion for selecting models for climate projections.

1. Introduction

The Fourth Assessment Report (AR4) of the Intergovernmental Panel on Climate Change (IPCC) treats climate projections from all models as a realization of equally credible possibilities. An important recognition going into the next assessment is that this may not be the best approach because some models are better in representing climate processes than others. A model ranking based on a skill metric or a selection process is, therefore, required [*Pierce et al.*, 2009]. The criteria for selection may be different depending on regions of interest, however it must be based on the correct simulation of the present-day climate, upon which, model performance can be benchmarked. The criterion must also be relevant; this means a systematic tendency toward a greater change in models in which a particular criterion is better met. In this study, we focus on whether the realism of simulating present-day IOD properties (e.g., in terms of its amplitude, and the associated rainfall teleconnection) has any relevance for future climate over the tropical IO and surrounding regions.

A positive IOD (pIOD) event refers to a pattern of SST variability occurring on interannual time scales in the equatorial IO [*Saji et al.*, 1999; *Webster et al.*, 1999; *Yu and Rienecker*, 1999] where ocean surface conditions are anomalously cool in the east and warm in the west. A pIOD event induces droughts in East Asia [*Guan and Yamagata*, 2003], southeast Australia [*Ummenhofer et al.*, 2009], Indonesia [*D'Arrigo and Smerdon*, 2008], and flooding to parts of India and East Africa (short rains) [*Black et al.*, 2003]. It also modulates the El Niño Southern Oscillation (ENSO)-monsoon relationship [*Ashok et al.*, 2001], and is linked to large outbreaks of major bushfires across southeast Australia. During 2002-2008 the IO experienced five pIOD events; these pIOD events form part of a long-term increase in pIOD frequency [*Cai et al.*, 2009a]. Based on 20th century experiments submitted to IPCC AR4, it is further shown that climate change contributes to the increasing frequency of pIOD occurrences [*Cai et al.*, 2009b]. Towards the end of the 21st century, a multi-model average projects a weaker warming rate over the eastern IO compared to the western IO (Figure 1a), along with a shallowing thermocline and increased easterly winds [*Vecchi and Soden*, 2007]. This partly contributes to a projected rainfall reduction over IOD-influenced regions such as southeast Australia (Figure 1b).

Given the potential ramifications of possible changes in IOD properties, are climate projections contingent on the "realism" of the present-day model IOD simulations? Should climate projections consider how well climate models simulate present-day IOD properties? We use inter-model variations to address these issues.

2. Data and Models

We take outputs of one experiment for a 50 year period (1950-1999) from each of the available 23 climate models that formed part of the Coupled Model Intercomparison Project Phase 3 (CMIP3). Outputs of SST, rainfall, wind and thermocline anomalies are linearly detrended and interpolated onto a common grid ($0.8° \times 1.9°$). The IOD properties diagnosed from the detrended data are taken to represent the present-day climate. The outputs are stratified into seasons, although we focus on austral spring (September to November, or SON), when an IOD event peaks.

The IOD is described through Empirical Orthogonal Function (EOF) analysis on SST anomalies in the tropical IO domain (15°S-15°N, 40°E-110°E). The IOD index is taken as the time series associated with the EOF spatial pattern, and has a standard deviation of one. The variance is expressed in the EOF spatial pattern, and its amplitude ($Amp(k)$, with k representing the 23 models) is calculated as the standard deviation of this spatial pattern. A positive value of the IOD index refers to a phase when SST anomalies are anomalously cold in the eastern IO (i.e., pIOD event). The modelled IOD amplitudes are compared to that calculated from a reconstructed Hadley Centre SST reanalysis product (HadISST) [*Rayner et al.*, 2003].

For future climate, we use outputs from 21st century CMIP3 experiments. Future rainfall changes ($\Delta Rain(x, y, k)$, k representing the 23 models) are expressed in terms of percentage change in climatology per degree of global warming (% $^{\circ}C^{-1}$). Likewise, future surface temperature changes ($\Delta Temp(x, y, k)$) are expressed in terms of °C per °C of global warming. We explore the linkage between future changes and the present-day simulation of the IOD amplitude.

3. The relevance of simulated IOD properties

If the IOD amplitude is relevant to future climate changes, then a model that simulates a greater amplitude should produce a greater change such that a fit, linear or otherwise, of the inter-model variations is statistically significant. This is a "necessary condition" that must be met, from which, physical processes may be identified.

Figure 2a plots inter-model variations of the present-day IOD amplitude versus projected surface temperature changes averaged over the eastern IO region (0-10°S, 100°E-110°E). The relevance of the IOD amplitude is underscored by a tendency for models with a greater amplitude to produce a smaller warming in the eastern IO. Taking each model as an independent sample, for 23 models, a linear fit requires an absolute correlation greater than 0.41 to be statistically significant at the 95% confidence level. The linear fit in Figure 2a is indeed statistically significant with a correlation of -0.47. The correlation of the linear fit is equivalent to that obtained by correlating $Amp(k)$ with $\Delta Temp(x, y, k)$ (with respect to k) averaged over the region. The significant correlation suggests that simulation of the IOD amplitude is relevant to the response of the east IO region to projections of temperature changes. Such relevance is also seen in projected rainfall changes over the same region (Figure 2b). Models with a greater IOD amplitude tend to produce a greater rainfall reduction over the eastern IO region.

The above linear fit analysis can be conducted for each grid point, by correlating $\Delta Temp(x, y, k)$(or $\Delta Rain(x, y, k)$) with the present-day IOD amplitude, $Amp(k)$, with respect to k. Maps of correlation coefficients for temperature and rainfall are plotted in Figures 2c and 2d. Again, models with a greater IOD amplitude produce a smaller warming rate over the eastern IO, with a greater corresponding rainfall reduction, extending to southeast Australia. These patterns are well-defined, suggesting that the relevance seen in Figures 2a and 2b is systematic. Given that most models simulate an overly strong IOD amplitude (Figure 2a) the projected rainfall reduction over southeastern Australia may be overestimated.

In terms of projections of surface temperature, the relevance is mainly confined to the ocean around Sumatra-Java (Figure 2c), but in terms of rainfall projections the relevance extends to land, particularly to regions where the IOD has an impact, like Indonesia. The IOD amplitude also has a strong relevance in rainfall projections over northern Australia

(Figure 2d). On inter-annual time scales, the IOD influences rainfall over these regions through the coherence with ENSO, although in most models the coherence is weaker than the observed [*Cai et al.*, 2009c]. During an El Niño event, which often occurs in conjunction with a pIOD episode, convection over the western Pacific decreases as the Walker circulation weakens and shifts westward. Under global warming, the Walker circulation is projected to weaken [*Vecchi and Soden*, 2007]. In models with a greater ENSO amplitude, and hence a greater IOD amplitude [*Cai et al.*, 2009c], the simulated reduction in the Walker circulation is stronger (see Figure 7 of *Cai et al.* [2010]). As a result, the rainfall reduction over these regions is also more pronounced. In regions outside northern Australia, the ENSO-IOD coherence has little relevance.

How is the relevance of the IOD amplitude to rainfall projections achieved? To this end, we investigate whether models with a stronger present-day IOD-rainfall teleconnection systematically produce a bigger rainfall reduction in the IOD-impacted regions. The present-day IOD-rainfall teleconnection is defined as the regression of detrended grid-point rainfall onto the IOD index (mm day^{-1} per unit of the IOD index). This teleconnection, measured by the regression coefficient, is ascribed as $TC(x, y, k)$ (k representing the 23 models). *Cai et al.* [2009c] show that the greater the IOD amplitude, the better the IOD-rainfall teleconnection is manifested. The teleconnection means that during pIODs rainfall over the eastern IO region decreases, indicated by a negative regression coefficient (Figure 3a).

Point-to-point correlation between $TC(x, y, k)$ and $\Delta Rain(x, y, k)$ (with respect to k) shows that models with a greater amplitude of the negative regression coefficient do systematically produce a greater rainfall reduction over much of the IOD-affected regions (Figure 3b), such as the Sumatra-Java and southeast Australia. Thus, the relevance of the IOD amplitude on rainfall projections are conducted through the IOD-rainfall teleconnection already operating in the present-day climate.

4. Mechanism for the relevance of the IOD amplitude

Previous studies [e.g., *Saji et al.*, 2006] have shown that most climate models simulate a Bjerknes-like positive feedback involving anomalous SSTs, winds, and the thermocline in the eastern IO [*Saji et al.*, 1999; *Webster et al.*, 1999], essential for the development of an IOD event. In response to increasing greenhouse gases, several factors may trigger a "perturbation" to the eastern IO circulation where the positive feedback operates. Firstly, a weakening of the Walker circulation generates easterly wind trends in the equatorial IO with a shoaling thermocline trend in the eastern IO [*Vecchi and Soden*, 2007]. Secondly, a greater warming over the surrounding land masses relative to the ocean generate similar wind trends [*Cai et al.*, 2009b], or dynamically support the wind trends associated with the weakening Walker circulation. It follows that models with a stronger positive feedback will generate a greater response to such perturbations.

The strength of the positive feedback in each model may be measured by the "sensitivity" of anomalies of zonal winds and the thermocline (defined as the 20°C isotherm, or Z20) to each model's IOD index obtained by a linear regression. The zonal wind-to-IOD and Z20-to-IOD sensitivity within each model may be referred to as $ZW{\Rightarrow}IOD(x, y, k)$ and $Z20{\Rightarrow}IOD(x, y, k)$ (k representing the 23 models), and they carry an unit of Nm^{-2} $^{\circ}C^{-1}$ and m $^{\circ}C^{-1}$, respectively. Figures 4a and 4b plot the inter-model variations of the IOD amplitude versus the zonal wind-to-IOD-sensitivity and Z20-to-IOD sensitivity averaged over the east IO region. We see that models with a greater IOD amplitude do systematically produce a greater sensitivity, which indicates a greater strength of the positive feedback. In both plots, the absolute correlation of the linear fit is greater than that required for statistical significance at the 95% confidence level (greater than 0.41).

To examine the spatial coherence of this inter-model relationship, the correlation and slope of such inter-model linear fits are calculated at each grid-point. This is equivalent to correlating $Amp(k)$ with $ZW{\Rightarrow}IOD(x, y, k)$, or regressing $ZW{\Rightarrow}IOD(x, y, k)$ onto $Amp(k)$, both with respect to k. The regression coefficients carry a unit of $Nm^{-2}\,{}^{\circ}C^{-2}$ and $m\,{}^{\circ}C^{-2}$, respectively. Maps of the correlations and regression slopes reveal that the inter-model relationship is spatially well-organised and well-defined, and strongest in the eastern IO, where the positive feedback operates. Models with a greater IOD amplitude (therefore with a greater positive feedback) produce a greater easterly wind-to-IOD sensitivity over the equatorial eastern IO but a greater westerly wind-to-IOD sensitivity to the south, reflecting a greater "anti-cyclonic circulation-to-IOD" sensitivity in models with a greater IOD amplitude. Consistently, models with a greater IOD amplitude, hence stronger positive feedback, display a greater Z20-to-IOD sensitivity, with a greater "thermocline shoaling-to-IOD" sensitivity over the equatorial eastern IO, but a stronger "thermocline deepening-to-IOD" sensitivity in the southern off-equatorial IO.

In general, these patterns of correlation and regression coefficients are reminiscent of the IOD anomaly patterns in individual models that describe the positive feedback [*Saji et al.*, 1999; *Webster et al.*, 1999]. It is this resemblance that underpins the relevance of the IOD amplitude to the magnitude of the eastern IO response to perturbations provided by climate change signals such as a weakening Walker circulation.

5. Conclusions

This study addresses whether simulated IOD properties of the present-day climate are relevant to such inter-model variations in the projected climate. We show that models with greater IOD amplitude systematically produce a smaller warming in the eastern IO, where a Bjerknes-like positive feedback operates involving SSTs, winds and the thermocline. Further, models with a greater IOD amplitude systematically produce a greater rainfall change in IOD-affected regions, projecting onto a stronger IOD-rainfall teleconnection that already operates in the present-day. We find that these results arise because models with a greater IOD amplitude possess a stronger Bjerknes-like positive feedback. As global warming continues into the 21st century, changes such as the easterly wind trends over the east IO associated with a weakening Walker circulation provide a perturbation, inducing a greater response in models with a greater IOD amplitude (hence a stronger positive feedback). As the climate change-induced perturbation is in the form of easterly wind trends, the response in the eastern IO is a slowdown of the warming rate. An important conclusion is that simulation of the IOD properties of the present-day climate can influence future climate; therefore, this study emphasizes the importance of bench-marking IOD simulation in selecting models for future climate projections. Given that most models produce an IOD amplitude greater than the observed, it is likely the projected changes are overly large. Our result strengthens the argument that some models should carry a greater weight when conducting multi-model averages of projected changes to the regional climate.

Acknowledgments.

We thank Peter van Rensch and Vassili Kitsios for their useful points of discussion which greatly benefited the manuscript. We also thank the two anonymous reviewers for their comments and suggestions.

References

Ashok, K., Z. Guan, and T. Yamagata (2001), Impact of the Indian Ocean Dipole on the relationship between the Indian Monsoon rainfall and ENSO, *Geophys. Res. Lett.*, *28*, 4499—4502.

Black, E., J. Slingo, and K. R. Sperber (2003), An observational study of the relationship between excessively strong short rains in coastal East Africa and Indian Ocean SST, *Mon. Wea. Rev.*, *131*, 74—94.

Cai, W., T. Cowan, and A. Sullivan (2009a), Recent unprecedented skewness towards positive Indian Ocean Dipole occurrences and its impact on Australian rainfall, *Geophys. Res. Lett.*, *36*, L11705, doi:10.1029/2009GL037604.

Cai, W., A. Sullivan, and T. Cowan (2009b), Climate change contributes to more frequent consecutive positive Indian Ocean Dipole events, *Geophys. Res. Lett.*, *36*, L23704, doi: 10.1029/2009GL040163.

Cai, W., A. Sullivan, and T. Cowan (2009c), Rainfall teleconnections with Indo-Pacific variability in the WCRP CMIP3 models, *J. Climate*, *22*(19), 5046–5071.

Cai, W., T. Cowan, J. Ribbe, G. Shi, and A. Sullivan (2010), Are anthropogenic aerosols responsible for the northwest Australia summer rainfall increase? A CMIP3 perspective and implications, *J. Climate*, (conditionally accepted).

D'Arrigo, R., and J. E. Smerdon (2008), Tropical climate influences on drought variability over Java, Indonesia, *Geophys. Res. Lett.*, *35*, L05707, doi:10.1029/2007GL032589.

Guan, Z., and T. Yamagata (2003), The unusual summer of 1994 in East Asia: IOD teleconnections, *Geophys. Res. Lett.*, *30*, 1544, doi:10.1029/2002GL016831.

Pierce, D. W., T. P. Barnett, B. D. Santer, and P. J. Gleckler (2009), Selecting global climate models for regional climate change studies, *Proc. Nat. Acad. Sci.*, *106*(21), 8441–8446.

Rayner, N. A., D. E. Parker, E. B. Horton, C. K. Folland, L. Alexander, D. P. Rowell, E. C. Kent, and A. Kaplan (2003), Global analyses of sea surface temperature, sea ice, and night marine air temperature since the late nineteenth century, *J. Geophys. Res.*, *108(D14)*, 4407, doi:10.1029/2002JD002670.

Saji, N. H., B. N. Goswami, P. N. Vinayachandran, and T. Yamagata (1999), A dipole mode in the tropical Indian Ocean, *Nature*, *401*, 360–363.

Saji, N. H., S.-P. Xie, and T. Yamagata (2006), Tropical Indian Ocean variability in the IPCC twentieth-century climate simulations, *J. Climate*, *19*, 4397—4417.

Ummenhofer, C. C., M. H. England, P. C. McIntosh, G. A. Meyers, M. J. Pook, J. S. Risbey, A. S. Gupta, and A. S. Taschetto (2009), What causes Southeast Australia's worst droughts?, *Geophys. Res. Lett.*, *36*, L04706, doi:10.1029/2008GL036801.

Vecchi, G. A., and B. J. Soden (2007), Global warming and the weakening of the tropical circulation, *J. Climate*, *20*, 4316—4330.

Webster, P. J., A. M. Moore, J. P. Loschnigg, and R. R. Leben (1999), Coupled ocean-atmosphere dynamics in the Indian Ocean during 1997-98, *Nature*, *401*, 356–360.

Yu, L., and M. M. Rienecker (1999), Mechanisms for the Indian Ocean warming during the 1997-98 El Niño, *Geophysical Research Letters*, *26*(6), 735–738.

Figure 1. Average over 23 models of SON trends in (a) surface temperature (°C per °C of global warming), and (b) rainfall (% change per °C of global warming).

Figure 2. Inter-model variations in IOD amplitude of the present-day climate versus variations in (a) future surface temperature changes (°C per °C of global warming) and (b) rainfall changes(% change per °C of global warming)at an east IO grid point (100°E, 3°S). The observed IOD amplitude as calculated from HadISST is shown as a vertical red line. Maps of correlation, with respect to the models, (c) between IOD amplitude of the present-day climate ($Amp(k)$) and grid-point surface temperature changes ($\Delta Temp(x, y, k)$), and (d) between IOD amplitude of the present-day climate ($Amp(k)$) and grid-point rainfall changes ($\Delta Rain(x, y, k)$).

Figure 3. (a) Inter-model variations of IOD-Rainfall teleconnection of the present-day climate versus future rainfall changes (% per °C of global warming) at an east IO grid point (100°E, 3°S). (b) Map of point-to-point correlation between IOD-rainfall teleconnection ($TC(x, y, k)$) and future rainfall changes ($\Delta Rain(x, y, k)$), with respect to the models (k).

Figure 4. Inter-model variations of IOD amplitude versus the sensitivity to the IOD of (a) zonal wind and (b) Z20 averaged over the east IO region (region). The observed IOD amplitude as calculated from HadISST is shown as a vertical red line. (c) Map of regression coefficients (colour, in $Nm^{-2}\ {}^{\circ}C^{-2}$) obtained by regressing grid-point zonal wind-to-IOD sensitivity, $ZW{\Rightarrow}IOD(x, y, k)$ ($Nm^{-2}\ {}^{\circ}C^{-1}$) onto IOD amplitude $Amp(k)$ (with respect to k). Superimposed are correlations between $ZW{\Rightarrow}IOD(x, y, k)$ and $Amp(k)$, again with respect to k (only contours representing statistical significance at the 95% confidence level are shown). (d) The same as (c) but for the thermocline-to-IOD sensitivity ($Z20{\Rightarrow}IOD(x, y, k)$) regressions coefficients ($m\ {}^{\circ}C^{-2}$).

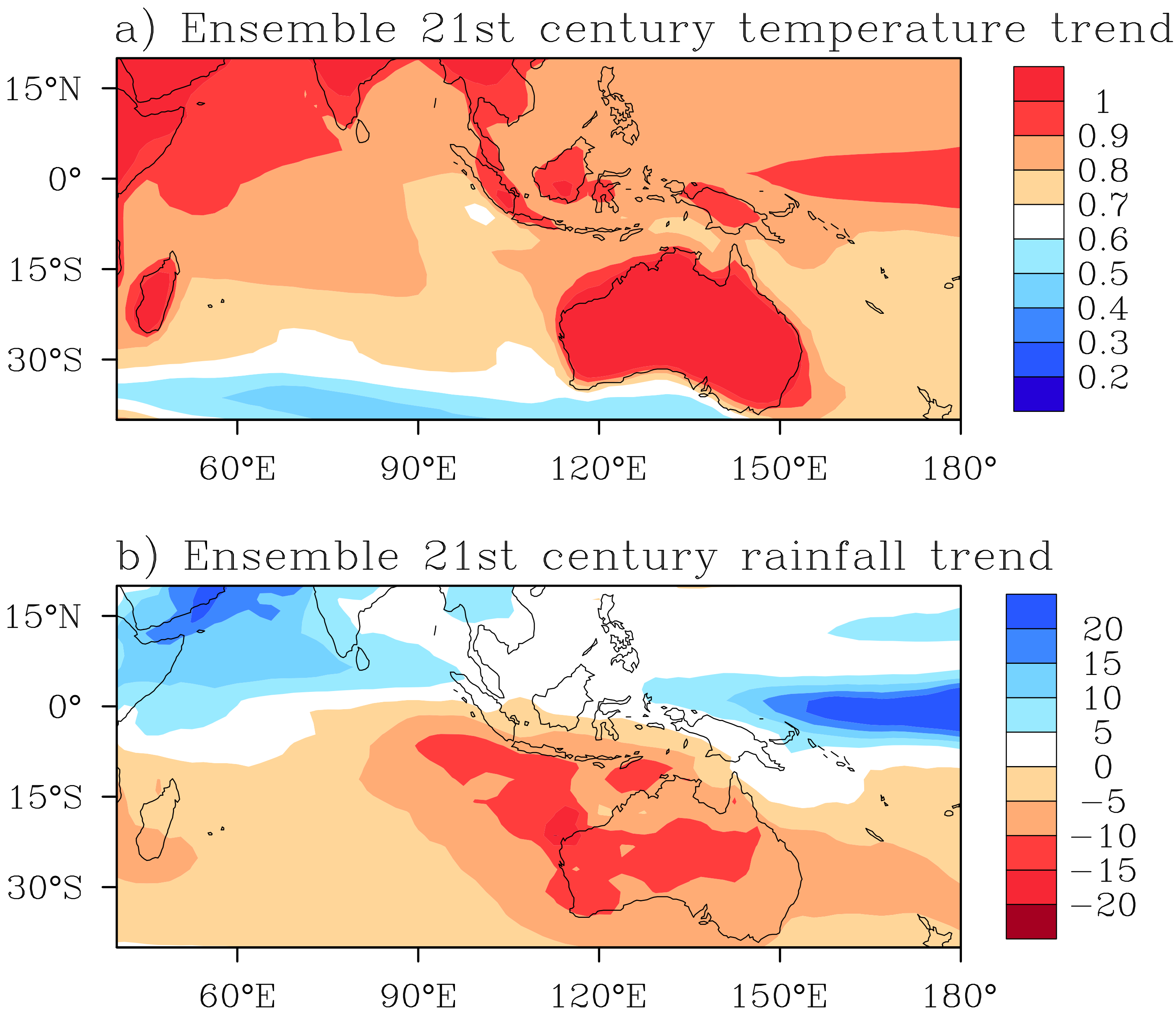
a) Ensemble 21st century temperature trend
15°N
0°
15°S
30°S
60°E
90°E
120°E
150°E
180°
1
0.9
0.8
0.7
0.6
0.5
0.4
0.3
0.2
b) Ensemble 21st century rainfall trend
15°N
0°
15°S
30°S
60°E
90°E
120°E
150°E
180°
20
15
10
5
0
−5
−10
−15
−20

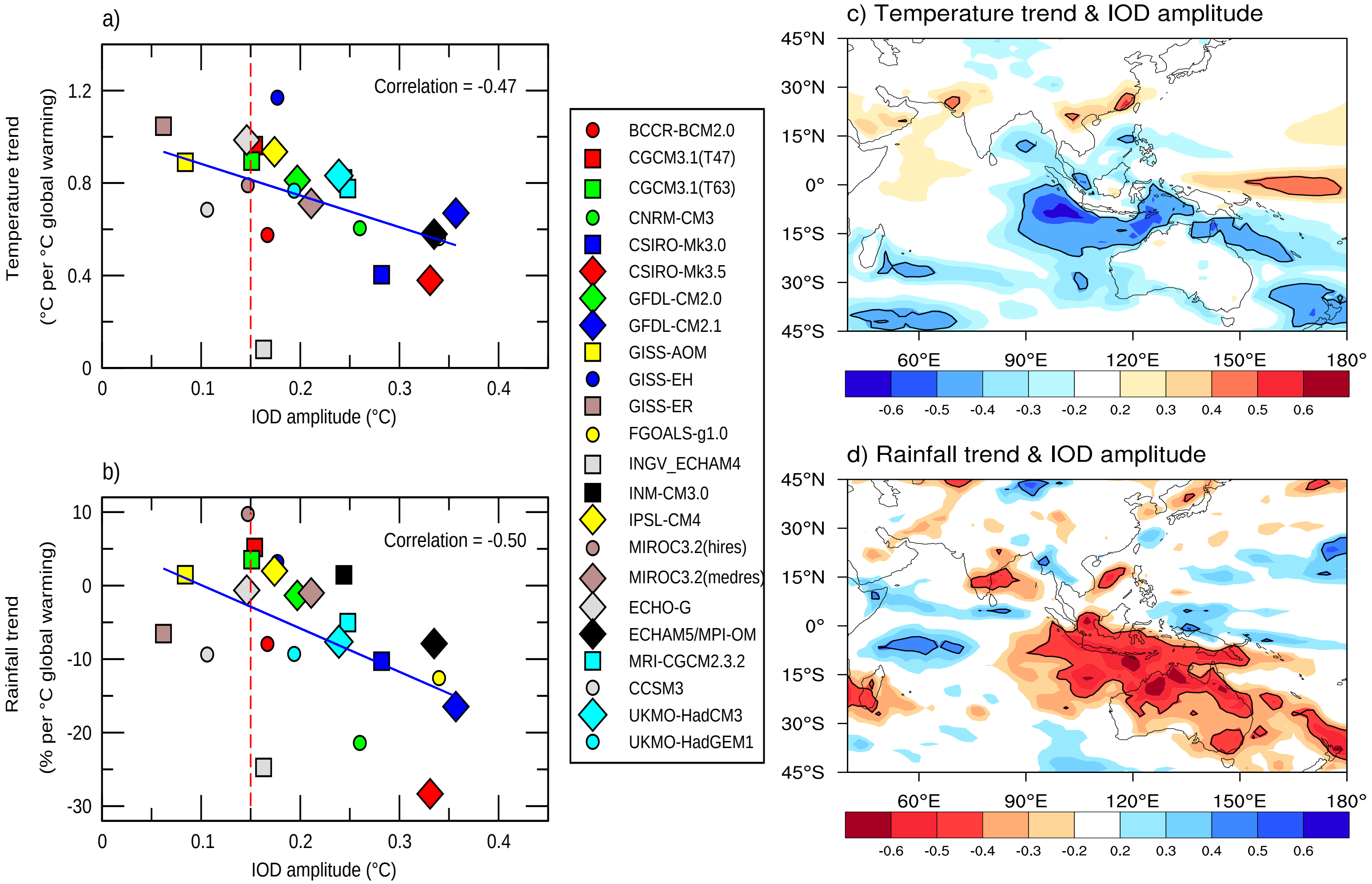

a)
Temperature trend
(°C per °C global warming)
Correlation = -0.47
IOD amplitude (°C)
b)
Rainfall trend
(% per °C global warming)
Correlation = -0.50
IOD amplitude (°C)
BCCR-BCM2.0
CGCM3.1(T47)
CGCM3.1(T63)
CNRM-CM3
CSIRO-Mk3.0
CSIRO-Mk3.5
GFDL-CM2.0
GFDL-CM2.1
GISS-AOM
GISS-EH
GISS-ER
FGOALS-g1.0
INGV_ECHAM4
INM-CM3.0
IPSL-CM4
MIROC3.2(hires)
MIROC3.2(medres)
ECHO-G
ECHAM5/MPI-OM
MRI-CGCM2.3.2
CCSM3
UKMO-HadCM3
UKMO-HadGEM1
c) Temperature trend & IOD amplitude
d) Rainfall trend & IOD amplitude
45°N
30°N
15°N
0°
15°S
30°S
45°S
60°E
90°E
120°E
150°E
180°
-0.6
-0.5
-0.4
-0.3
-0.2
0.2
0.3
0.4
0.5
0.6

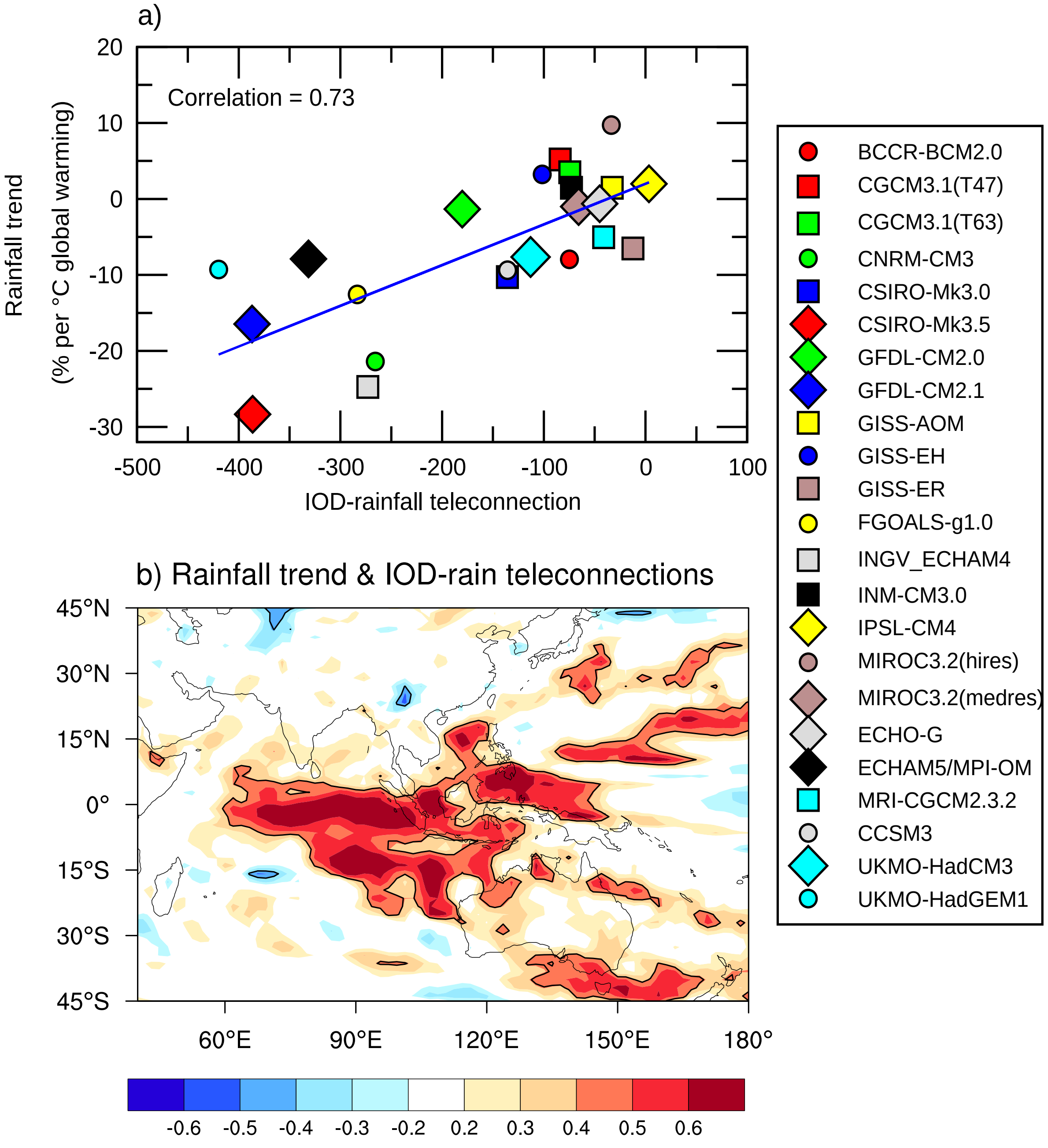
a)
Correlation = 0.73
Rainfall trend
(% per °C global warming)
20
10
0
-10
-20
-30
-500
-400
-300
-200
-100
0
100
IOD-rainfall teleconnection
BCCR-BCM2.0
CGCM3.1(T47)
CGCM3.1(T63)
CNRM-CM3
CSIRO-Mk3.0
CSIRO-Mk3.5
GFDL-CM2.0
GFDL-CM2.1
GISS-AOM
GISS-EH
GISS-ER
FGOALS-g1.0
INGV_ECHAM4
INM-CM3.0
IPSL-CM4
MIROC3.2(hires)
MIROC3.2(medres)
ECHO-G
ECHAM5/MPI-OM
MRI-CGCM2.3.2
CCSM3
UKMO-HadCM3
UKMO-HadGEM1
b) Rainfall trend & IOD-rain teleconnections
45°N
30°N
15°N
0°
15°S
30°S
45°S
60°E
90°E
120°E
150°E
180°
-0.6
-0.5
-0.4
-0.3
-0.2
0.2
0.3
0.4
0.5
0.6

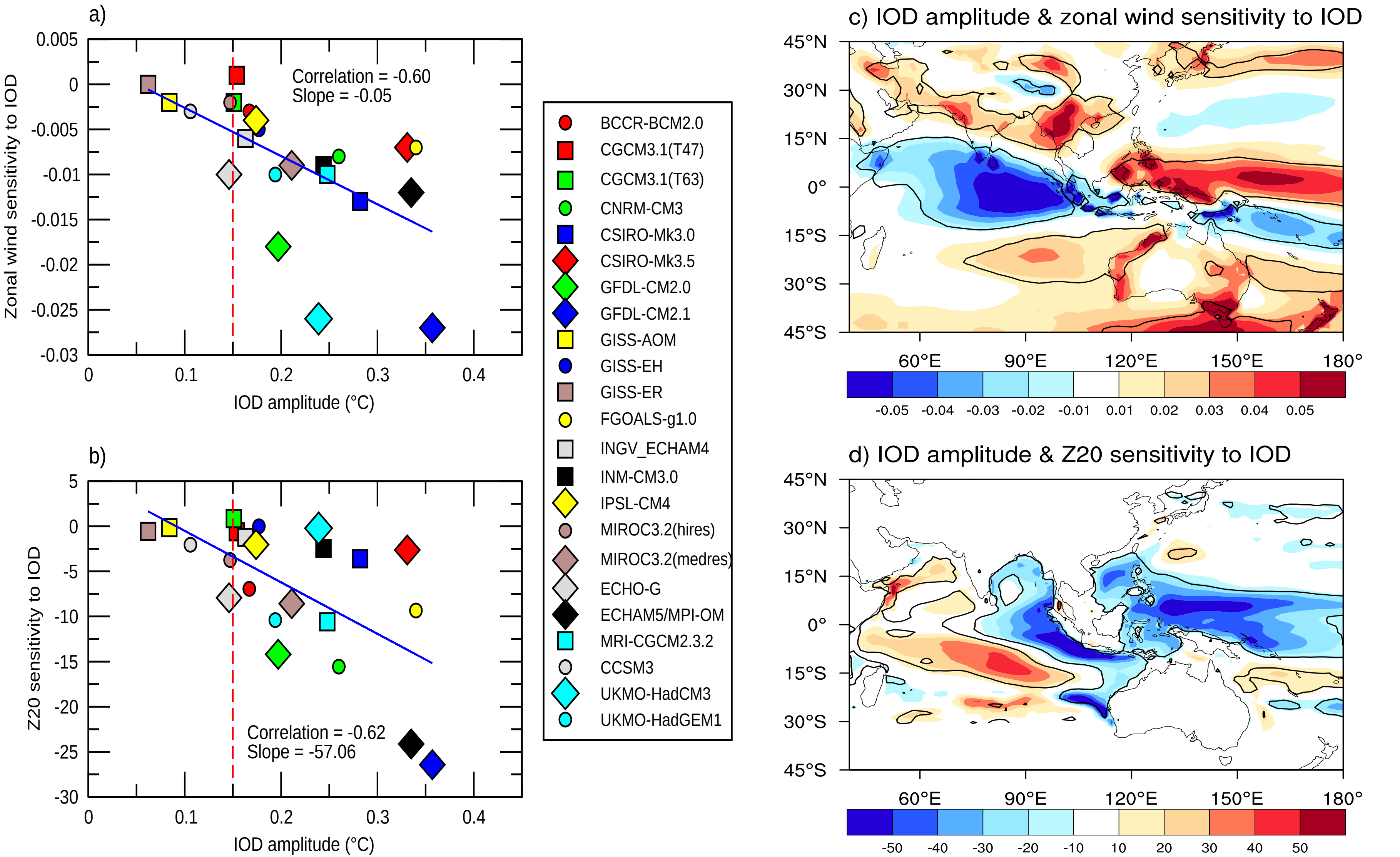
a)
Correlation = -0.60
Slope = -0.05
Zonal wind sensitivity to IOD
IOD amplitude (°C)
b)
Correlation = -0.62
Slope = -57.06
Z20 sensitivity to IOD
IOD amplitude (°C)
BCCR-BCM2.0
CGCM3.1(T47)
CGCM3.1(T63)
CNRM-CM3
CSIRO-Mk3.0
CSIRO-Mk3.5
GFDL-CM2.0
GFDL-CM2.1
GISS-AOM
GISS-EH
GISS-ER
FGOALS-g1.0
INGV_ECHAM4
INM-CM3.0
IPSL-CM4
MIROC3.2(hires)
MIROC3.2(medres)
ECHO-G
ECHAM5/MPI-OM
MRI-CGCM2.3.2
CCSM3
UKMO-HadCM3
UKMO-HadGEM1
c) IOD amplitude & zonal wind sensitivity to IOD
d) IOD amplitude & Z20 sensitivity to IOD